ELSEVIER

Stability of a compressible hydrous melt layer above the transition zone

Bryony A.R. Youngs, David Bercovici *

Department of Geology and Geophysics, Yale University, New Haven, CT, USA

ARTICLE INFO

ABSTRACT

Seismic and mineral physics structures suggest melt can be generated at the top of the transition zone. Because the melt phase is significantly more compressible than the solid phase, it is expected that a density crossover occurs with increasing pressure. Experimental studies suggest this crossover lies towards the base of the upper mantle. If the density crossover lies above the 410 km discontinuity, melt will collect and form a layer until such time as it reaches the crossover when part of it may become unstable. We investigate the stability of a compressible melt layer which intersects the density crossover. Analytic models of instabilities are used to determine the effects of compressibility and crossover location on instability growth rates. We find that increasing the compressibility increases growth rates due to the fact that rising perturbations expand and become more unstable as they rise. If the density crossover lies above a melt layer at the transition zone, perturbations must be large before becoming unstable, making it likely that the layer would remain. However, when the density crossover lies within the melt layer, all perturbations are unstable and they drain the melt layer completely unless diapiric separation occurs.

1. Introduction

Upwelling mantle material ascending through the Earth's transition zone into the upper mantle can potentially undergo dehydration melting (Inoue, 1994). This effect is a consequence of the water solubility contrast between transition zone minerals and those of the upper mantle. Ringwoodite and Wadsleyite, the principal components of the transition zone, have solubilities at least an order of magnitude higher than that of olivine, the main upper mantle mineral (Kohlstedt et al., 1996). Consequently, when the system is in equilibrium, the transition zone water concentration will be higher than that of the upper mantle (Bolfan-Casanova et al., 2000; Richard et al., 2002). For a sufficiently high mantle water content the transition zone will have a water concentration higher than the water storage capacity (solubility or solidus limit, depending on the temperature) of the upper mantle resulting in ascending material being 'super-saturated' on leaving the transition zone (Huang et al., 2006), which leads to partial melting. There is evidence to suggest this process occurs in some locations; in particular seismic studies have detected a low velocity zone in some areas just above the 410-km discontinuity, which could be interpreted as a layer of partial melt (Revenaugh and Sipkin, 1994; Song et al., 2004; Courtier and Revenaugh, 2007).

A question remains as to the fate of melt at the 410-km discontinuity. In many instances melt is less dense than its solid counterpart

and, if this were the case, melt generated at the 410-km discontinuity would rise into the upper mantle. However, mineral physics experiments suggest that dry silicate melts are more dense than their solid phases at the pressures at the base of the upper mantle (Stopler et al., 1981; Agee and Walker, 1988; Ohtani et al., 1995; Agee, 2007); this results from the fact that the melt phase is more compressible than the solid phase and hence its density increases more rapidly with depth. The addition of water decreases both the melt density and its incompressibility, although for small enough water concentrations, hydrous melts are also expected to be stable just above the transition zone (Matsukage et al., 2005; Sakamaki et al., 2006). The density crossover, where the melt ceases to be gravitationally stable, is likely to lie close to the base of the upper mantle (Ohtani and Maeda, 2001). In this case it is possible to form a melt layer which rests on top of the 410-km discontinuity.

The Transition Zone Water Filter Model (Bercovici and Karato, 2003) hypothesizes that partial melting at the 410-km discontinuity can filter out incompatible elements such as uranium and thorium into the melt phase. Melt which rests on the 410-km discontinuity can then be entrained back into the lower mantle (Bercovici and Karato, 2003; Leahy and Bercovici, 2007) thereby recycling the incompatible elements. The model provides a mechanism for sustaining distinct chemical reservoirs and apparent layering within a whole mantle convection system. A crucial aspect of the Transition Zone Water Filter Model is that the melt layer be denser than the solid so that incompatible elements do not escape into the upper mantle MORB source region.

Clearly a melt layer which lies entirely beneath the density crossover will always be stable whereas if the density crossover lies beneath

* Corresponding author.
  E-mail address: david.bercovici@yale.edu (D. Bercovici).

the 410 km discontinuity melt generated at the top of the transition zone will not be stable and no melt layer will form. Given that the density crossover is thought to lie towards the base of the upper mantle it is entirely possible that a melt layer at the 410-km discontinuity may intersect the density crossover and be partially unstable. Here we construct simple mathematical models to understand the stability and evolution of such a melt layer. The aim is to address the question of how having an unstable portion of the melt layer affects the stability of the layer as a whole and under what conditions a significant amount of melt would be lost into the upper mantle. From our models we are able to predict the growth rates of any instabilities and establish how they vary with the location of the density crossover and physical properties of the melt.

2. Mathematical model

2.1. Formulation

We consider the problem of a thin melt layer overlain by a much thicker solid layer. The system is modelled in 2D as a thin, compressible layer beneath an incompressible half-space (Fig. 1). The melt occupies the region $z=0$ to $z=h$ where the height of the layer, h, can be expressed as the sum of the average layer height, h_a, and a perturbation, δh:

$$h(x, t) = h_a + \delta h(x, t) \tag{1}$$

The flow within both layers is assumed to be viscous creeping and consequently the system obeys the Stokes equation:

$$\nabla \cdot \boldsymbol{\tau} - \nabla p + \rho \boldsymbol{g} = 0 \tag{2}$$

where p denotes pressure, ρ density, g gravitational acceleration and the components of the viscous stress tensor, $\boldsymbol{\tau}$, are given by

$$\tau_{ij} = \eta \left(\frac{\partial u_i}{\partial x_j} + \frac{\partial u_j}{\partial x_i} \right) + \eta_2 \frac{\partial u_k}{\partial x_k} \delta_{ij} \tag{3}$$

where $\boldsymbol{u} = (u, w)$ is the velocity field, η is the dynamic viscosity and η_2 the second viscosity.

Assuming all viscosities are constant and substituting Eq. (3) in Eq. (2) gives

$$\eta \nabla^2 \boldsymbol{u} + (\eta + \eta_2) \nabla (\nabla \cdot \boldsymbol{u}) - \nabla p + \rho \boldsymbol{g} = 0. \tag{4}$$

Given that the lower layer is melt and the overlying layer is solid, we assume $\eta_s \gg \eta_m$ where the subscript s denotes the overlying solid layer and m the melt layer. Thus, the upper layer acts as a rigid boundary for the lower layer while the lower layer acts as a free-slip boundary for the upper layer. The boundary conditions on the velocity field can be summarised by

$$\text{on } z = 0 : u_m = 0 \tag{5a}$$

$$\text{on } z = h : u_m = 0 \tag{5b}$$

$$\text{on } z = h : \frac{\partial u_s}{\partial z} + \frac{\partial w_s}{\partial x} = 0 \tag{5c}$$

$$\text{as } z \to \infty : u_s \to 0 \text{ and } w_s \to 0. \tag{5d}$$

There must also be continuity of vertical velocity and normal stress on the interface between the fluids, i.e.:

$$\text{on } z = h : w_s = w_m = \frac{\partial h}{\partial t} \tag{6}$$

$$\delta \sigma_{zz}^s = \delta \sigma_{zz}^m + \Theta(\delta h) \tag{7}$$

incompressible solid layer

$z = h$

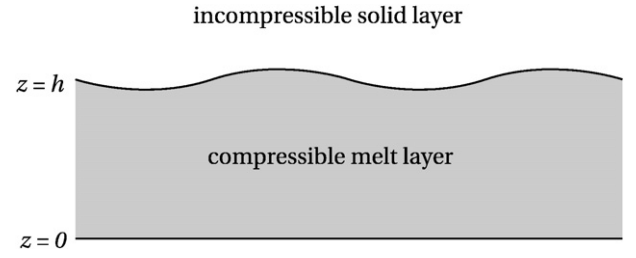compressible melt layer

$z = 0$

Fig. 1. Schematic diagram of the 2D model.

where $\delta \sigma_{zz}$ represents the deviation in normal stress from the hydrostatic background value (the superscripts indicate whether it is calculated on the upper or lower side of the interface) and

$$\Theta(\delta h) = \int_{h_a}^{h_a + \delta h} (\rho_m - \rho_s) g \, dz \tag{8}$$

is the pressure difference induced by a hydraulic head of height δh.

2.2. Melt layer density profile

The density and pressure in each layer may be written as the sum of a hydrostatic reference profile, which depends only on height z, and a perturbation that depends on the position vector x and time t:

$$p = p^*(z) + p'(x, t) \tag{9}$$

$$\rho = \rho^*(z) + \rho'(p', T') \tag{10}$$

where T' is the temperature perturbation. A key component of the model is the reference density profile assumed for the melt layer. Since the fluid in the overlying layer is incompressible, its reference density profile is simply a constant and is denoted ρ_s^*. In the melt layer, however, the density will decrease with increasing z-coordinate. The exact relationship depends on the assumed form of the bulk modulus, K:

$$K = \rho^* \frac{\partial p^*}{\partial \rho^*}. \tag{11}$$

The bulk modulus, a measure of a fluid's incompressibility, will increase with increasing pressure. The Murnaghan equation of state assumes that the bulk modulus increases linearly with pressure and is found to be a good approximation inside the Earth. Therefore, we write

$$K_m = K_0 + K' p_m^* \tag{12}$$

for positive constants K_0 and K'. Substituting this into Eq. (11) and knowing that the reference pressure must satisfy

$$\frac{\partial p_m^*}{\partial z} = -\rho_m^* g \tag{13}$$

we find that

$$\rho_m^* = \rho_0 \left(1 - \frac{K' - 1}{z_0} z \right)^{\frac{1}{K' - 1}}. \tag{14}$$

For the special case $K' = 1$ this becomes

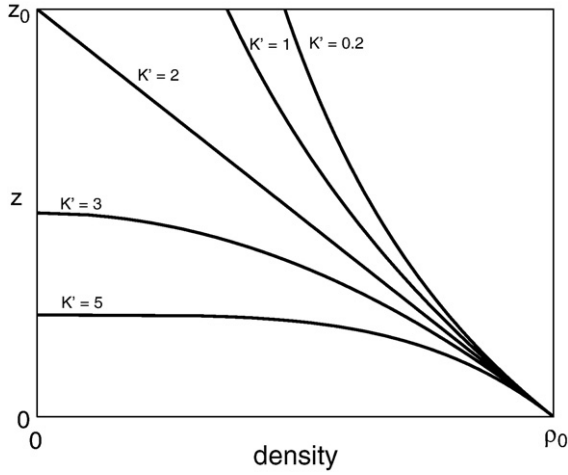$$\rho_m^* = \rho_0 e^{-\frac{z}{z_0}} \tag{15}$$

Fig. 2. Density as a function of vertical coordinate, z, for various values of K'. This graph assumes z_0 is a constant (see text).

where $\rho_0 = \rho_m^*(z=0)$ and z_0 is a length scale which is directly related to the incompressibility of the fluid. For $K'>1$, the equation of state model is invalid for heights $z>z_0/(K'-1)$ and we must confine our analysis well below this limit. For $0<K'<1$, $\rho_m^* \to 0$ as $z \to \infty$. Examples of density profiles for various values of K' are shown in Fig. 2. It should be noted that in the expression for ρ_m^* there are three constants: ρ_0, z_0 and K', of which only two can be set independently given a reference point for both the density and pressure. For example, if we assume $\rho_m^* = \rho_0$ and $p^* = p_0$ at $z=0$, then using

$$\frac{\partial \rho_m^*}{\partial z} = \frac{\partial \rho_m^*}{\partial p^*} \cdot \frac{\partial p_m^*}{\partial z} \tag{16}$$

we can calculate that

$$z_0 = \frac{K_0 + K'p_0}{\rho_0 g}. \tag{17}$$

The exact values of the constants in the melt and solid density profiles will determine the height of the density crossover, d, or vice-versa ($\rho_s^* = \rho_m^*(d)$). In general we assume melt is gravitationally stable at $z=0$ ($\rho_0 > \rho_s^*$).

2.3. Solution method

The equations are solved within each layer separately using boundary conditions on $z=0$, $z \to \infty$ and the interface $z=h$ Eqs. (5)–(7).

Since the upper layer is incompressible, satisfying $\nabla \cdot \boldsymbol{u}_s = 0$, Eq. (4) within this layer becomes

$$\eta_s \nabla^2 \boldsymbol{u}_s - \nabla p_s + \rho_s \boldsymbol{g} = 0. \tag{18}$$

Taking, respectively, the divergence and curl gives

$$\nabla^2 p_s = 0 \tag{19}$$

$$\nabla^4 \boldsymbol{\Psi}_s = 0 \tag{20}$$

where $\boldsymbol{u}_s = \nabla \times \boldsymbol{\Psi}_s$. Given that the flow field is 2-dimensional, $\boldsymbol{\Psi}_s = (0, \Psi_s, 0)$.

Conservation of mass within the lower layer is given by the general equation

$$\frac{\partial \rho_m}{\partial t} + \boldsymbol{u}_m \cdot \nabla \rho_m + \rho_m \nabla \cdot \boldsymbol{u}_m = 0. \tag{21}$$

The perturbation term of the density field can be written as

$$\rho_m' = \rho_m^*(\beta_m p_m' - \alpha_m T_m') \tag{22}$$

where $\beta = 1/K$ is the compressibility and α is the coefficient of thermal expansion. Using an assumption similar to the Boussinesq approximation, the perturbation term is neglected everywhere except in the momentum balance (justified as long as $\beta_m \rho_m'$ and $\alpha_m T_m'$ are small). We also assume the anelastic approximation, i.e. $\partial \rho_m/\partial t = 0$. Together these approximations are known as the anelastic-liquid approximation and imply (Jarvis and McKenzie, 1980)

$$\nabla \cdot \boldsymbol{u}_m = -\frac{w}{\rho_m^*} \frac{\partial \rho_m^*}{\partial z}. \tag{23}$$

Under the small-slope assumption for the lower layer, the x-component of Eq. (4) can be approximated by (Appendix A)

$$\eta_m \frac{\partial^2 u_m}{\partial z^2} - \frac{\partial p_m'}{\partial x} = 0. \tag{24}$$

Applying the boundary conditions, the velocity field can be written as

$$u_m = \frac{1}{2\eta_m} \frac{\partial p_m'}{\partial x} z(z-h). \tag{25}$$

Because the vertical velocity component is neglected within the melt layer, the normal stress on the lower side of $z=h$ can simply be expressed as

$$\delta \sigma_{zz}^m = -p_m' \tag{26}$$

which, with Eq. (7), can be used to obtain an expression for the melt layer pressure P_m' that can, in turn, be substituted into Eq. (25) to obtain the velocity within the lower layer.

3. Infinitesimal instabilities

The development of Rayleigh–Taylor instabilities has been well studied by previous authors when both fluids are incompressible (e.g. Whitehead and Luther, 1975; Ribe, 1998). We use similar analytic techniques to calculate the growth rates of infinitesimal instabilities to ascertain the effect of compressibility on the initial development of perturbations.

We assume that the interface perturbation from Eq. (1) can be written as

$$\delta h(x, t) = F(t) \cos kx \tag{27}$$

Given the boundary conditions (5)–(7) and the assumption that δh is small (allowing boundary conditions on $z=h$ to be evaluated on the constant surface $z=h_a$), the solutions to Eqs. (19) and (20) are

$$p_s' = Pe^{-kz} \cos kx \tag{28}$$

$$\Psi_s = (Q + Rz)e^{-kz} \sin kx \tag{29}$$

where

$$P = 2k\eta_s R \tag{30a}$$

$$Q = F'(t)e^{kh_a} \frac{(1-kh_a)}{k} \tag{30b}$$

$$R = F'(t)e^{kh_a} \tag{30c}$$

in which $F'(t) = dF/dt$. From this we can calculate the normal stress on the upper side of the $z = h$ boundary:

$$\delta\sigma_{zz}^s = \left[-p'_s + 2\eta_s \frac{\partial w_s}{\partial z}\right]_{z=h} \tag{31}$$

$$= -2\eta_s k \frac{\partial h}{\partial t}. \tag{32}$$

Under this assumption that δh is small, the hydraulic head function, Θ, may be approximated by

$$\Theta(\delta h) = \Delta\rho g \delta h \tag{33}$$

where $\Delta\rho = \rho_m^*(z = h_a) - \rho_s^*$, is the density difference between the melt at height h_a and the solid. This approximation allows for the pressure induced by a hydraulic head of finite height δh but neglects any density variation within the melt layer over this small distance.

The time dependent part of the density interface perturbation is assumed to take the form

$$F(t) = be^{at} \tag{34}$$

where b is small. Consequently, using Eq. (25), the velocity field within the melt layer may be written as

$$u_m = \frac{bk}{2\eta_m}(\Delta\rho g + 2k\eta_s a)e^{at}\sin kx \cdot z(h_a - z). \tag{35}$$

To obtain a relation for $\partial h/\partial t$ consider mass conservation within a vertical slice through the melt layer:

$$\int_0^h \frac{\partial}{\partial x}(\rho_m u_m)dz = -\rho_m(h)\frac{\partial h}{\partial t}. \tag{36}$$

Again we have assumed the anelastic-liquid and thin layer approximations. Substituting for u_m in this expression and rearranging gives us an expression for the growth rate, a:

$$a = \frac{-\Delta\rho g}{2k\eta_s + \frac{2\eta_m \rho_m^*(h_a)}{k^2 I(h_a)}} \tag{37}$$

where

$$I(h) = \int_0^h \rho_m z(h-z)dz \tag{38}$$

corresponds to the mass flux of fluid through a layer of height h. Note that the growth rate is positive for an unstable density interface ($\rho_m^*(z=h_a) < \rho_s^*$) and negative for a stable density interface. (In the incompressible limit, $I/\rho_m^* = h^3/6$ in which case Eq. (37) yields the classical growth rate given by Whitehead and Luther (1975).) Because the perturbations are assumed to be small their stability cannot change by reaching the density crossover. The magnitude of the growth rate depends on the wavenumber of the instability. The maximum growth rate is

$$a_{max} = -\frac{\Delta\rho g}{3\eta_s}\left(\frac{I(h_a)}{2\rho_m^*(h_a)}\right)^{1/3}\left(\frac{\eta_s}{\eta_m}\right)^{1/3} \tag{39}$$

and occurs at a wavenumber given by

$$k_{max}^3 = \frac{2\rho_m^*(h_a)\eta_m}{I(h_a)\eta_s}. \tag{40}$$

As an example we consider the case where $K' = 1$ as the density profile has an expression which can be integrated easily. Since the growth rate Eq. (37) trivially depends on the density contrast at the
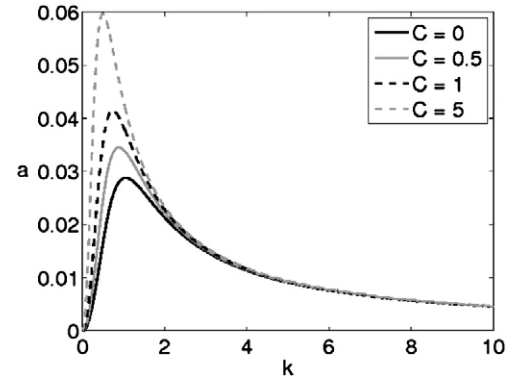

Fig. 3. Growth rate magnitude versus wavenumber for varying degrees of compressibility. $K' = 1$, $\eta_s/\eta_m = 10$, $\Delta\rho = -1$. The wavenumber k is scaled by $1/h_a$. Although the thin-layer approximation suggests that solutions are only valid for $kh_a < 1$, a full 2D development gives essentially identical results.

melt-solid interface, $\Delta\rho$, we hold this quantity constant (taken to be −1) and vary z_0 to determine the effect of an increasing degree of compressibility of the initial instability growth rate. Note that this means we are no longer free to specify ρ_0. Fig. 3 shows curves of growth rate versus wavenumber for varying degrees of compressibility. Here we have defined $C = 1/z_0$ which is directly related to how compressible the fluid is. Increasing the compressibility results in an increase in the growth rate magnitude. The difference is particularly noticeable around the maximum. The value of k where the maximum occurs also decreases slightly as the compressibility increases.

The only parameter in Eq. (37) which varies in these calculations is the mass flux of fluid, I (Eq. (38)). As the compressibility increases so does I due to the density increase with depth. Hence the difference in initial growth rate with compressibility can be explained by enhanced mass transport from beneath a downward perturbation to an upward perturbation.

It should be noted that Fig. 3 is plotted for a viscosity ratio $\eta_s/\eta_m = 10$. As this ratio increases the effect of compressibility on the growth will become less apparent for a fixed large k since the second term in the denominator of Eq. (37) becomes less significant. However, as η_s/η_m increases, the maximum growth rate increases and occurs at diminishing wavenumbers k (see Eqs. (39) and (40)); thus the least stable mode is in fact affected more by compressibility with increasing viscosity contrast.

4. Finite amplitude deformation

4.1. Model setup

In order to study the long term stability of the melt layer we must consider the development of finite amplitude instabilities. Following Bercovici and Kelly (1997) we have created a simple model whereby we assume that the interface undulates with a repeating pattern of crests and troughs. Rather than attempting to model the exact shape of these undulations we consider only the progression of their average height (defined to conserve mass beneath). Fig. 4 illustrates the main components of the model. The unperturbed layer height is h_a, the rising crest height is h_c and the descending trough height h_t. Flow within the layer is assumed to be in the horizontal direction only (thin layer approximation, Appendix A) and is confined beneath the base of the descending trough (i.e. beneath $z = h_a - h_t$). We do not model the entire pressure field but consider only the average pressure deviation from the reference field beneath the crest, p'_c, and the trough p'_t. For simplicity, and to focus on the effects of compressibility, the system is assumed to repeat with one period λ, although crests and troughs do not necessarily have the same widths (e.g., see Ribe, 1998).

The heights of the crests and troughs must satisfy the following conservation of mass equation:

$$\int_0^{h_a + h_c} \rho_m^* dz + \int_0^{h_a - h_t} \rho_m^* dz = 2 \int_0^{h_a} \rho_m^* dz \tag{41}$$

The velocity field within the melt layer is given by

$$u_m = \frac{1}{2\eta_m} \frac{\partial p'}{\partial x} z(z - h_a + h_t) \tag{42}$$

where in this case we assume

$$\frac{\partial p'}{\partial x} = \frac{p'_c - p'_t}{\lambda/2}. \tag{43}$$

Note this expression is for the pressure difference between two sections as shown in Fig. 4 where the trough is at a higher x-coordinate than the crest. When the positions are reversed there will be a sign change in this expression.

The flux of material from the trough section to the crest section, Q, is given by

$$Q = -\int_0^{h_a - h_t} \rho_m^* u_m dz = \frac{(p'_c - p'_t)}{\eta_m \lambda} I(h_a - h_t) \tag{44}$$

where I is as defined in Eq. (38). The total mass increase of the trough section and mass decrease of the crest section is twice this amount:

$$2Q = \frac{\lambda}{2} \rho_m^* (h_a + h_c) \frac{\partial h_c}{\partial t} \tag{45}$$

$$2Q = \frac{\lambda}{2} \rho_m^* (h_a - h_t) \frac{\partial h_t}{\partial t} \tag{46}$$

which gives

$$\rho_m^* (h_a + h_c) \frac{\partial h_c}{\partial t} = \rho_m^* (h_a - h_t) \frac{\partial h_t}{\partial t}. \tag{47}$$

This expression can also be obtained by differentiating Eq. (41) with respect to time. To solve exactly for the growth rates, $\partial h_c/\partial t$ and $\partial h_t/\partial t$, we use the normal stress balance Eq. (7) where, as before

$$\delta\sigma_{zz}^m = -p' \tag{48}$$

$$\delta\sigma_{zz}^s \alpha - \frac{\eta_s}{\lambda} \frac{\partial h_i}{\partial t} \tag{49}$$

with $i = c$ or t. The constant of proportionality in Eq. (49) could be determined exactly in the infinitesimal deflection case as the exact

shape of the boundary was known. Here it is expected to be similar to a sinusoidal boundary so we assume it is 4π as in Eq. (32). We obtain the flux, Q, from Eq. (44) by writing

$$p'_c - p'_t = \frac{4\pi\eta_s}{\lambda} \left(\frac{\partial h_c}{\partial t} + \frac{\partial h_t}{\partial t} \right) + \Theta(h_c) - \Theta(-h_t) \tag{50}$$

Combining Eqs. (44), (45) and (50) gives:

$$\frac{\partial h_c}{\partial t} \left[\frac{\rho_m^*(h_a + h_c)\eta_m \lambda^2}{4I(h_a - h_t)} + \frac{4\pi\eta_s}{\lambda} \left(1 + \frac{\rho_m^*(h_a + h_c)}{\rho_m^*(h_a - h_t)} \right) \right] = -(\Theta(h_c) - \Theta(-h_t)) \tag{51}$$

which gives $\partial h_c/\partial t$ as a function of h_c. $\partial h_t/\partial t$ can then be calculated from Eq. (47). We can compare the initial growth rates in this case with the results of Section 3 by considering Eq. (51) in the limit h_c, $ht \to 0$:

$$\frac{\partial h_c}{\partial t} = \left[\frac{-\Delta\rho g}{\frac{4\pi\eta_s}{\lambda} + \frac{\rho_m^*(h_a)\eta_m \lambda^2}{8I(h_a)}} \right] h_c. \tag{52}$$

The initial growth is exponential with a rate given by the bracketed term. This expression is almost identical to Eq. (37) although there is a slight difference in the coefficient of the second term in the denominator caused by the simplified form of the pressure gradients in this model. The maximum initial growth rate occurs when $\lambda = \lambda_{max}$ where

$$\lambda_{max}^3 = \frac{16\pi I(h_a)\eta_s}{\rho_m^*(h_a)\eta_m}. \tag{53}$$

4.2. Effects of compressibility

We use Eq. (51) to calculate the growth rates of finite amplitude perturbations for varying degrees of compressibility within the layer. For simplicity we use the melt layer density profile with $K' = 1$: $\rho_m^*(z) = \rho_0 e^{-Cz}$ where C is a measure of the magnitude of the compressibility. Similar effects will be seen for all values of K' although the exact magnitudes of growth involved will vary. For the calculations in this section densities are non-dimensionalised with respect to ρ_0, lengths with respect to the initial melt layer thickness, h_a and time with respect to $\eta_m/\rho_0 g h_a$. The instability wavelength is assumed to be λ_{max} (Eq. (53)). Since this is the wavelength of the fastest initial growth rate it is the instability wavelength which is most likely to occur. Recall that this wavelength varies with the magnitude of C. The overlying solid is assumed to be 100 times more viscous than the melt.

Firstly we apply this model to the case of an unstable and incompressible melt layer with an identical density contrast between the melt and solid at $z = h_a$ as used in the subsequent compressible
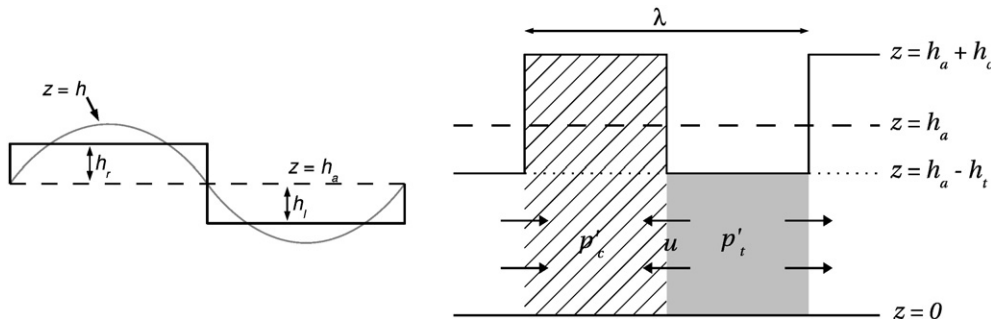

Fig. 4. Schematic model of finite amplitude deformation of the melt-solid interface. Left: The undulating interface is approximated by a box function. Right: The melt layer is divided into two regions: beneath the crest (denoted with a subscript c) and beneath the trough (denoted with a subscript t). The velocity field arrows assume the perturbations are unstable and the crests are rising and the troughs descending.
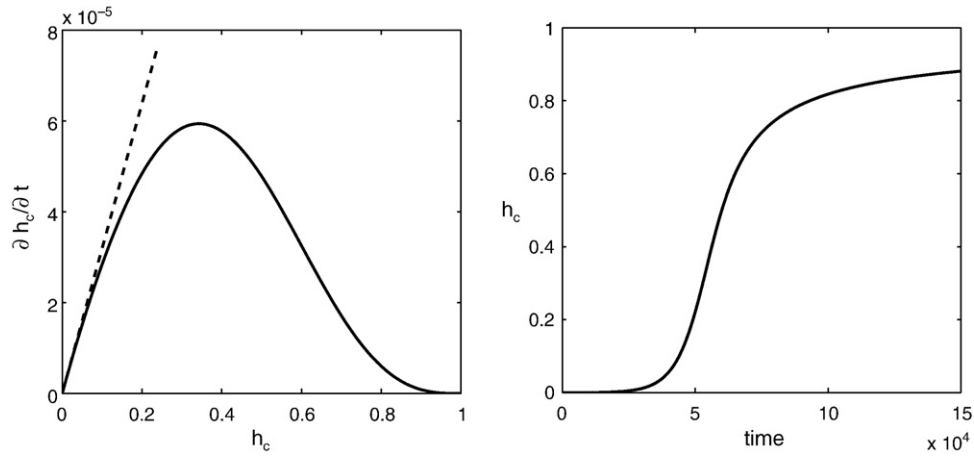
Fig. 5. Evolution of perturbations for an incompressible, unstable melt layer ($C=0$) with $\lambda=\lambda_{max}$ and $\eta_s/\eta_m=100$. Left: Growth rate, $\partial h_c/\partial t$, versus perturbation height, h_c. The dashed line indicates the initial exponential growth rate. Right: Perturbation height versus time.

calculation. In this case the heights of the crests, h_c, and troughs, h_t, will be identical at all times. Fig. 5 shows how the growth rate of the crest and trough height evolves. The growth rate slows from the initial exponential growth due to the trough descending and constricting the channel through which material can flow. Eventually the trough reaches the base of the layer and the growth rates fall to zero as the fluid flow channel is completely drained. The rising crest achieves its maximum height which, in this case, is equal to the layer thickness, h_a.

In Section 3 we saw that compressibility increased the initial growth rates of instabilities due to the increased ease of mass transfer from beneath the descending troughs to beneath the rising crests. With our finite deformation model we ascertain the effects of compressibility on finite amplitude growth rates and in particular answer the question of what happens to an instability which intersects the density crossover. We now consider the case where the melt layer is unstable at $z=h_a$ but where the density crossover occurs within the melt layer such that the base of the layer is stable. If the density crossover occurs at a height d above the base of the melt layer, where $0<d<h_a$, then the density of the overlying solid must be $\rho_s=\rho_0 e^{-Cd}$. For a melt layer that is compressible, the height of the rising crest is greater than that of the descending trough. Moreover, because the crests inflate from decompressing they will become more unstable as they rise

which will act to increase growth rates; similarly the troughs will become less unstable as they descend (due to compression) and eventually become stable when they reach the density crossover which should act to reduce growth rates.

Fig. 6 shows the evolution of growth rates for $C=0.5$ and $d=0.8$, from which it is clear that the introduction of compressibility has increased the growth rates moderately. The increased instability of rising crests is a larger effect than the increased stability of descending troughs. As before, constriction of the fluid flow channel eventually causes growth of the perturbations to terminate. However, the maximum height attained by the crests is now larger than the initial layer thickness. These results suggest that a partially stable compressible melt layer may not be sufficient to prevent its drainage as rising instabilities from the unstable portion drag material from the entire layer.

4.3. Critical compressibility

In some cases the rising crests are not able to drain the melt layer completely. When the compressibility is above a certain critical value the descending troughs are able to balance crests of any permitted height without ever reaching the base of the layer. Consider the mass
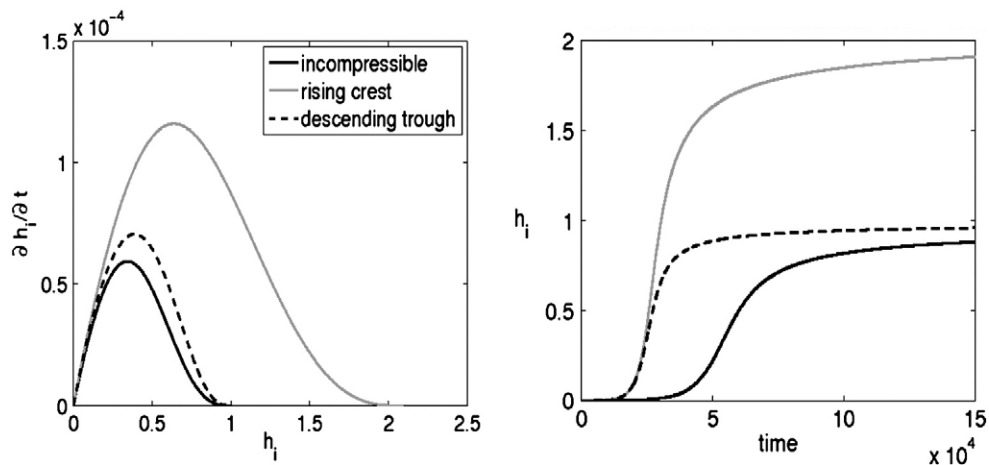

Fig. 6. Evolution of perturbations for a compressible melt layer with $Ch_a=0.5$, $K'=1$, $\lambda=\lambda_{max}$ and $\eta_s/\eta_m=100$. Left: Growth rate, $\partial h_i/\partial t$ versus perturbation height, h_i. Right: Perturbation height versus time.

conservation Eq. (41) in the special case where the troughs have reached $z=0$:

$$\int_{h_a}^{h_a+h_c} \rho_m^*(z)dz = \int_0^{h_a} \rho_m^*(z)dz \tag{54}$$

which becomes

$$2\left(1-\frac{K'-1}{z_0}h_a\right)^{\frac{K'}{K'-1}}-1 = \left(1-\frac{K'-1}{z_0}(h_a+h_c)\right)^{\frac{K'}{K'-1}} \tag{55}$$

and in the special case $K'=1$

$$2e^{-\frac{h_a}{z_0}}-1 = e^{-\frac{h_a+h_c}{z_0}}. \tag{56}$$

The right-hand side of both Eqs. (55) and (56) must always be positive, thus the compressibility parameter $C=1/z_0$ must satisfy

$$Ch_a < \frac{1-\left(\frac{1}{2}\right)^{\frac{K'-1}{K'}}}{K'-1} \tag{57}$$

which, in the case $K'=1$, is equivalent to

$$Ch_a < \ln 2. \tag{58}$$

If the magnitude of the compressibility exceeds these critical values the melt layer will not drain completely. This has significant implications for the growth rates of the rising crests. As they are no longer limited by constriction of the fluid flow channel they continue to increase as the crest rises, a phenomenon we term *runaway growth*. Fig. 7 shows the growth rate for $K'=1$ and a value of C above the critical compressibility. While the descending trough has a maximum height which is less than h_a, the crest continues to rise indefinitely with the growth rate steadily increasing.

When $K'>1$ growth of the perturbations must stop when they reach height $z=z_0$. Even for $K'\leq1$ there would, in reality, be some height (for example, the Earth's surface) above which the perturbations cannot rise. However, if the compressibility is above the critical value it is these external factors, rather than drainage of the melt layer, which limit the maximum height attained by the crest. It should be noted that it is mass conservation, not stability induced by crossing the density crossover, which prevents the troughs from reaching the base of the melt layer when the compressibility is super-critical.
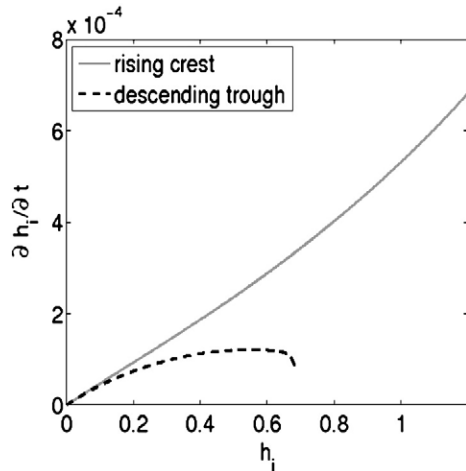

Fig. 7. Evolution of perturbations for a compressible melt layer with $Ch_a=1.0$, $K'=$, $\lambda=\lambda_{max}$ and $\eta_s/\eta_m=100$. Plot shows growth rate, $\partial h_i/\partial t$ versus perturbation height, h_i.
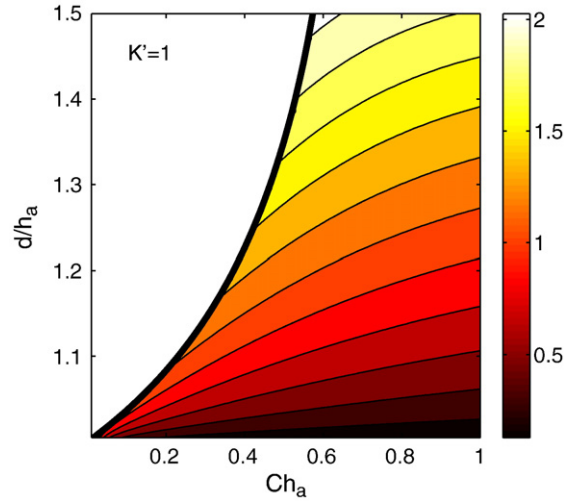

Fig. 8. Contour plot of the height above the density crossover of the smallest unstable perturbation as a function of the density crossover height, d, and the compressibility parameter, C, for $K'=1$. All quantities have been non-dimensionalised with respect to the unperturbed melt layer thickness, h_a.

4.4. Stable melt layer

Another question which can be addressed using our simple finite deformation model is the fate of a melt layer which lies entirely beneath the density crossover when unperturbed. Clearly small interface deflections which do not reach the density crossover will be stable with negative growth rates. However, there will be some perturbation height above which the growth rates become positive and the perturbation unstable. From Eq. (51):

$$\text{sign}\left(\frac{\partial h_c}{\partial t}\right) = \text{sign}(\Theta(-h_t)-\Theta(h_c)). \tag{59}$$

From this we can calculate the smallest value of h_c for which the growth rate is positive. When the density crossover lies within the melt layer the growth rate is positive for all values of h_c. When the density crossover lies above the melt layer the smallest unstable perturbation height depends on both the position of the density crossover and the magnitude of the compressibility.

Fig. 8 shows how high above the density crossover a perturbation must be in order to be unstable for the case $K'=1$. The thick black line marks the point above which there are no solutions and all perturbations are stable. For values in this unshaded region, even at the maximum possible value of h_c, which occurs when the channel has drained completely beneath a trough, the growth rate is still negative. This black line asymptotes to the critical value of Ch_a, in this case $\ln 2$. If Ch_a is above the critical value, and the perturbation height is not limited by mass conservation, we always obtain a solution.

There are two expected effects which are evident from Fig. 8. Firstly, as the height of the density crossover increases, so does the height above this density crossover that a perturbation must have before it becomes unstable. Secondly, as the magnitude of the compressibility parameter increases, the height of unstable perturbations decreases. When the fluid is more compressible, density changes occur more rapidly and hence a smaller height of unstable fluid above the density crossover is necessary to balance the stable column of fluid below it.

5. Discussion

5.1. Earth-like parameters

Analysis of our simple model can help us understand the fate of a compressible melt layer that lies close to the density crossover. In
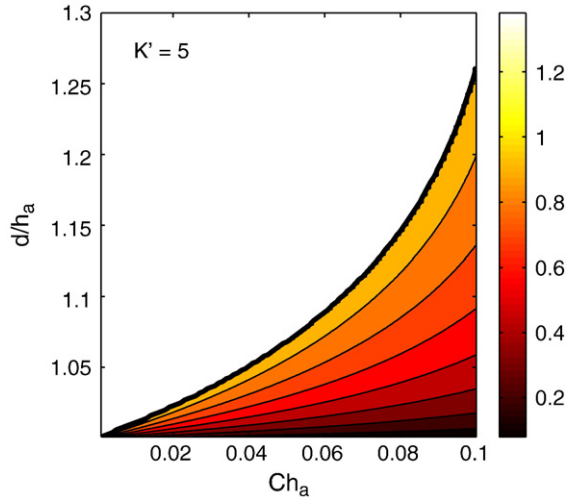
Fig. 9. Contour plot of the height above the density crossover of the smallest unstable perturbation as a function of the density crossover height, d, and the compressibility parameter, C, for $K' = 5$. All quantities have been non-dimensionalised with respect to the unperturbed melt layer thickness, h_a.

order to determine what happens to a melt layer above the transition zone we must obtain estimates of the parameters involved under conditions at the base of the upper mantle. Mineral physics experiments suggest that hydrous silicate melt has a bulk modulus derivative with respect to pressure of $K' \sim 5$ and density at the top of the transition zone of $\rho_0 \sim 3.3 \times 10^3$ kg m^{-3} (Matsukage et al., 2005; Sakamaki et al., 2006). The exact values of K' and ρ_0 depend on the water content of the melt. Assuming the pressure at the top of the transition zone is $p_0 \sim 13$ GPa we can use Eq. (17) to calculate $z_0 \sim 2 \times 10^6$ m and $C \sim 5 \times 10^{-7}$ m^{-1}. The bulk modulus at zero pressure, K_0, is assumed to be negligible compared to $K' p_0$.

There are two possibilities to consider: the density crossover lying within the melt layer or lying a small distance above the melt layer. In the first instance perturbations are always unstable but the height which they may reach without diapiric separation and their ability to drain the entirety of the melt layer depends on the magnitude of Ch_a relative to the critical value. Below the critical value rising crests are able to drain the whole melt layer beneath the troughs; once this happens there is no more material to supply the rising crests, hence their growth terminates and they eventually succumb to diapiric separation (e.g., Bercovici and Kelly, 1997). Above the critical value of Ch_a rising crests will extend indefinitely whilst beneath troughs the melt layer will never drain completely. From Eq. (57) we can calculate that the critical value of Ch_a for $K' = 5$ is 0.10. Since a melt layer at the 410-km discontinuity is likely to be no more than several tens of kilometers thick, we can be reasonably confident that the Earth's system lies comfortably within the sub-critical domain.

For a density crossover which lies above the melt layer the stability of perturbations is shown in Fig. 9. A melt layer between 10 km and 100 km thick has corresponding Ch_a values of 0.005 and 0.05. Hence realistic Earth values lie on the far left of this figure. In this instance the density crossover must lie very close to the top of the melt layer for it to even be possible for any perturbations to be unstable. If this is satisfied, perturbations that are a significant fraction of the melt layer thickness are necessary before they are unstable. This suggests that if the melt layer lies entirely beneath the density crossover when unperturbed it will be stable to nearly all, if not all, perturbations.

5.2. Conclusions

The Transition Zone Water Filter Model requires a melt layer above the 410 km discontinuity to be gravitationally stable. These results indicate that the average melt layer height must remain below the

density crossover for this to happen. We saw in the previous section that even if the melt layer lies only just beneath the density crossover perturbations must be large before they become unstable. In contrast, as soon as the unperturbed layer height reaches the density crossover the layer is unstable to all perturbations and these perturbations will drain the melt layer completely.

Existence of the density crossover part way through the melt layer is not sufficient to ensure that part of the layer remains stable. However, the initial growth rates of instabilities are directly proportional to the density contrast at the melt-solid interface. Therefore, the closer the density crossover is to the melt-solid interface, the slower the growth rates will be. If the density crossover lies sufficiently close to the top of the melt layer it is possible that, even though instabilities will grow indefinitely, they may take geologically long periods of time to develop. Dimensionalising the time-scale in Fig. 6 we find that the instabilities take on the order of several tens of millions of years to develop for a density crossover at $0.8h_a$, indicating that unstable perturbations indeed take geologically long periods of time to form.

The above analysis assumes that the rising instabilities remain attached to the melt layer at all times. In practice a rising perturbation will separate from the melt layer if its Stokes (or free ascent) velocity exceeds its growth rate (Whitehead and Luther, 1975; Bercovici and Kelly, 1997). After this happens it is possible that the remaining layer will lie entirely beneath the density crossover and hence be stable. Consequently, even if rising perturbations have the potential to completely drain the melt layer, separation may occur and prevent this from happening.

Appendix A. Thin layer approximation in compressible fluids

The x-direction component of the momentum Eq. (4) within the melt layer is given by

$$\left(2\eta_m + \eta_{2m}\right)\frac{\partial^2 u_m}{\partial x^2} + \left(\eta_m + \eta_{2m}\right)\frac{\partial^2 w_m}{\partial z \partial x} + \eta_m \frac{\partial^2 u_m}{\partial z^2} - \frac{\partial p_m}{\partial x} = 0. \tag{A.1}$$

This can be simplified considerably under the assumption that the layer is thin (i.e. $\delta x \gg \delta z$). Firstly,

$$\frac{\partial^2 u_m}{\partial x^2} \ll \frac{\partial^2 u_m}{\partial z^2} \tag{A.2}$$

so the first term of Eq. (A.1) can be neglected.

We can express the velocity field in terms of a mass flux vector, $\boldsymbol{J}$, multiplied by specific volume, V_r:

$$u_m = V_r J_x \quad \text{and} \quad w_m = V_r J_z \quad \text{where} \quad V_r = \frac{1}{\rho_m(z)} \tag{A.3}$$

where $\nabla \cdot \boldsymbol{J} = 0$. Considering the second term of Eq. (A.1) in terms of $\boldsymbol{J}$ and V_r, we can write

$$\frac{\partial^2 w_m}{\partial x \partial z} = \frac{\partial J_z}{\partial x} \cdot \frac{\partial V_r}{\partial z} - V_r \frac{\partial^2 J_x}{\partial x^2} \tag{A.4}$$

The second term in this relation is small since it scales as $1/\delta x^2$. Using the fact that $\nabla \cdot \boldsymbol{J} = 0$ we can obtain a scaling relationship for J_z:

$$J_z \sim -H\frac{\partial J_x}{\partial x} \tag{A.5}$$

where H is a typical layer thickness. Therefore,

$$\frac{\partial J_z}{\partial x} \sim -\frac{\partial H}{\partial x} \cdot \frac{\partial J_x}{\partial x} - H\frac{\partial^2 J_x}{\partial x^2} \tag{A.6}$$

Both terms scale as $1/\delta x^2$ so $\partial J_z/\partial x$ is small. Also,

$$\frac{\partial V_r}{\partial z} \sim \frac{V_r}{L} \tag{A.7}$$

where L is a typical scale height for the density profile. Since $L \gg H$ this expression will never be large. Consequently the second term of Eq. (A.1) can also be neglected and the equation can be written as

$$\eta_m \frac{\partial^2 u_m}{\partial z^2} - \frac{\partial p_m}{\partial x} = 0 \tag{A.8}$$

The z-direction component of Eq. (4) within the melt layer is given by

$$\left(2\eta_m + \eta_{2m}\right) \frac{\partial^2 w_m}{\partial z^2} + \left(\eta_m + \eta_{2m}\right) \frac{\partial^2 u_m}{\partial z \partial x} + \eta_m \frac{\partial^2 w_m}{\partial x^2} - \frac{\partial p_m}{\partial z} - \rho_m g = 0 \tag{A.9}$$

As before,

$$\frac{\partial^2 w_m}{\partial x^2} \ll \frac{\partial^2 w_m}{\partial z^2} \tag{A.10}$$

so the third term can be neglected.
From Eq. (A.8)

$$\eta_m \frac{\partial u_m}{\partial z} \sim H \frac{\partial p_m}{\partial x} \tag{A.11}$$

Therefore

$$\eta_m \frac{\partial^2 u_m}{\partial x \partial z} \sim \frac{\partial}{\partial x} \left(H \frac{\partial p_m}{\partial x}\right) \ll \frac{\partial p_m}{\partial z} \text{ or } \rho_m g \tag{A.12}$$

and hence can be neglected. Finally,

$$\left(2\eta_m + \eta_{2m}\right) \frac{\partial^2 w_m}{\partial z^2} = \left(2\eta_m + \eta_{2m}\right) \frac{\partial}{\partial z^2} \left(V_r J_z\right)$$
$$= -\left(2\eta_m + \eta_{2m}\right) \frac{\partial^2}{\partial x \partial z} \left(V_r J_z\right) + \left(2\eta_m + \eta_{2m}\right) \frac{\partial}{\partial z} \left(\frac{\partial V_r}{\partial z} J_z\right) \tag{A.13}$$

The first term on the right side of Eq. (A.13) is of the same order as Eq. (A.12) which has already been shown to be small. From Eqs. (A.5) and (A.7) one can show that

$$\frac{\partial}{\partial z} \left(\frac{\partial V_r}{\partial z} J_z\right) \sim -\frac{H}{L} \frac{\partial^2}{\partial x \partial z} \left(V_r J_x\right) \tag{A.14}$$

which when multiplied by $(2\eta_m + \eta_{2m})$ is also small compared to $\partial p_m / \partial z$ and $\rho_m g$. Therefore, Eq. (A.9) can be written as

$$\frac{\partial p_m}{\partial z} + \rho_m g = 0. \tag{A.15}$$

References

Agee, C.B., 2007. Static compression of hydrous silicate melt and the effect of water on planetary differentiation. Earth Planet. Sci. Lett. 265, 641–654.

Agee, C.B., Walker, D., 1988. Static compression and olivine flotation in ultrabasic silicate liquid. J. Geophys. Res. 93, 3437–3449.

Bercovici, D., Karato, S., 2003. Whole-mantle convection and the transition-zone water filter. Nature 425, 39–44.

Bercovici, D., Kelly, A., 1997. The non-linear initiation of diapirs and plume heads. Phys. Earth Planet. Inter. 101, 119–130.

Bolfan-Casanova, N., Keppler, H., Rubie, D., 2000. Water partitioning between nominally anhydrous minerals in the MgO–SiO$_2$–H$_2$O system up to 24 GPa: implications for the distribution of water in the Earth's mantle. Earth Planet. Sci. Lett. 182, 209–221.

Courtier, A.M., Revenaugh, J., 2007. Deep upper mantle melting beneath the Tasman and Coral seas detected with SCS reverberations. Earth Planet. Sci. Lett. 259, 66–76.

Huang, X., Xu, Y., Karato, S., 2006. Water content in the transition zone from electrical conductivity of wadsleyite and ringwoodite. Nature 434, 746–749.

Inoue, T., 1994. Effect of water on melting phase relations and melt composition in the system Mg$_2$SiO$_3$–H$_2$O up to 15 GPa. Phys. Earth Planet. Inter. 85, 237–263.

Jarvis, G.T., McKenzie, D.P., 1980. Convection in a compressible fluid with infinite Prandtl number. J. Fluid Mech. 96 (3), 515–583.

Kohlstedt, D., Keppler, H., Rubie, D., 1996. Solubility of water in the α, β, and γ phases of (Mg,Fe)$_2$SiO$_4$. Contrib. Mineral. Petrol. 123, 345–357.

Leahy, G., Bercovici, D., 2007. On the dynamics of a hydrous melt layer above the transition zone. J. Geophys. Res. 112 (B07401). doi:10.1029/2006JB004631.

Matsukage, K., Jing, Z., Karato, S., 2005. Density of hydrous silicate melt at the conditions of the Earth's deep upper mantle. Nature 438, 488–491.

Ohtani, E., Maeda, M., 2001. Density of basaltic melt at high pressure and stability of the melt at the base of the lower mantle. Earth Planet. Sci. Lett. 193, 69–75.

Ohtani, E., Nagata, Y., Suzuki, A., Kato, T., 1995. Melting relations of peridotite and the density crossover in planetary mantles. Chem. Geol. 120, 207–221.

Revenaugh, J., Sipkin, S., 1994. Seismic evidence for silicate melt atop the 410-km mantle discontinuity. Nature 369, 474–476.

Ribe, N.M., 1998. Spouting and planform selection in the Rayleigh–Taylor instability of miscible viscous fluids. J. Fluid Mech. 377, 27–45.

Richard, G., Monnereau, M., Ingrin, J., 2002. Is the transition zone an empty water reservoir? Inferences from numerical models of mantle dynamics. Earth Planet. Sci. Lett. 205 (1-2), 37–51.

Sakamaki, T., Suzuki, A., Ohtani, E., 2006. Stability of hydrous melt at the base of the Earth's upper mantle. Nature 439, 192–194.

Song, T., Helmberger, D., Grand, S., 2004. Low-velocity zone atop the 410-km seismic discontinuity in the northwestern United States. Nature 427, 530–533.

Stopler, E., Walker, D., Hager, B., Hays, J., 1981. Melt segregation from partially molten source regions: the importance of melt density and source region size. J. Geophys. Res. 86, 6261–6271.

Whitehead, J.A., Luther, D.S., 1975. Dynamics of laboratory diapir and plume models. J. Geophys. Res. 80, 705–717.